Remote Sensing of Environment 155 (2014) 325–333

Contents lists available at ScienceDirect

Remote Sensing of Environment

journal homepage: www.elsevier.com/locate/rse

Comparison of four types of 3D data for timber volume estimation

Johannes Rahlf [a,*], Johannes Breidenbach [a], Svein Solberg [a], Erik Næsset [b], Rasmus Astrup [a]

[a] Norwegian Forest and Landscape Institute, National Forest Inventory, P.O. Box 115, NO-1431 Ås, Norway
[b] Norwegian University of Life Sciences, Department of Ecology and Natural Resource Management, P.O. Box 5003, NO-1432 Ås, Norway

ARTICLE INFO

Article history:
Received 10 February 2014
Received in revised form 27 August 2014
Accepted 30 August 2014
Available online 27 September 2014

Keywords:
Forest inventory
Timber volume
Airborne laser scanning
Digital aerial photographs
Digital photogrammetry
TanDEM-X
TerraSAR-X
Radargrammetry
Mixed effects models

ABSTRACT

The study compares the accuracy of timber volume prediction based on four different three-dimensional remote sensing data sets in one study area in southern Norway: airborne laser scanning (ALS), stereo aerial photogrammetry (AP), satellite interferometric synthetic aperture radar (InSAR) based on the TanDEM-X mission, and satellite radargrammetry based on the TerraSAR-X mission. We fitted linear mixed effects models with vegetation height and density metrics obtained from the remote sensing data sets as explanatory variables. The cross-validated root mean squared error (RMSE) relative to the observed mean was used as the measure of goodness-of-fit. ALS provided the most accurate prediction at plot level with RMSE = 19%, followed by AP (31%), InSAR (42%), and radargrammetry (44%). At stand level the methods' performances were equally ordered, with RMSE values of 12–23%. Including the variables terrain slope and aspect in the models improved the accuracy of AP, InSAR, and radargrammetry slightly.

1. Introduction

Remote sensing data are often used for forest parameter prediction or to provide wall-to-wall information (mapping). In this way remote sensing can provide useful information for forest inventories. Common fields of application are stratification and small area estimation where remote sensing data serve as auxiliary variables to improve the precision of estimates.

Particularly three-dimensional (3D) remote sensing data contain useful information for forest inventories. Canopy height measurements obtained by remote sensing show a strong correlation with the product of height and density of vegetation, which is proportional to important forest characteristics such as biomass and timber volume (Treuhaft & Siqueira, 2000).

Especially airborne laser scanning (ALS) has been in the focus of research for the last two decades and is used today in operational forest inventories (e.g., Maltamo & Packalen, 2014; McRoberts, Tomppo, & Næsset, 2010; Næsset, 2014; Næsset et al., 2004). Besides measuring the surface elevation, a sufficient portion of the ALS beams penetrates the canopy and provides measurements taken from the forest floor. Such echoes can be used to create a digital terrain model (DTM), which is needed to calculate the measurements' height above ground. Due to large mapping campaigns in recent years, the coverage with accurate DTMs has increased in many countries. These accurate DTMs are used to derive the height above ground of forest canopies from other 3D remote sensing data.

Stereo aerial photogrammetry (AP) is a technique to derive 3D information from overlapping aerial photographs taken from different positions. While AP has been used in forestry for several decades (e.g., Hugershoff, 1933), recent developments in image matching and computing power have led to its renaissance in forest inventory research. Photogrammetry with a fully digital, automated work flow is also known as 3D vision (Leberl et al., 2010). Early studies applying 3D vision showed the suitability of AP data for forest parameter prediction (Næsset, 2002a; Schardt, Hruby, Hirschmugl, Wack, & Franke, 2004). Järnstedt et al. (2012) found that AP has a great potential for estimating and updating forest information, when comparing AP and ALS for their ability to estimate different forest parameters in Finland. In southern Germany, Straub, Stepper, Seitz, and Waser (2013) estimated plot-level attributes from AP data in mixed species forest and identified improvements by stratified estimation. Bohlin, Wallerman, and Fransson (2012) and Nurminen, Karjalainen, Yu, Hyyppä, and Honkavaara (2013) achieved similar accuracies with AP as with ALS-based methods for test sites in Sweden and Finland, respectively. AP data as well as fused AP and ALS data have been used for small area estimation by Breidenbach and Astrup (2012) and Steinmann, Mandallaz, Ginzler, and Lanz (2013).

Synthetic aperture radar (SAR) is another prominent remote sensing technique that can provide 3D data. Four methods to generate 3D data from SAR exist (Toutin & Gray, 2000): interferometry (InSAR),

* Corresponding author.
E-mail address: jor@skogoglandskap.no (J. Rahlf).

http://dx.doi.org/10.1016/j.rse.2014.08.036
0034-4257/

radargrammetry, clinometry, and polarimetry. Whereas airborne systems often have a higher spatial resolution, satellite systems can cover larger areas. Forest parameters have been successfully predicted and estimated with both airborne SAR systems (Neeff, Dutra, dos Santos, da Costa Freitas, & Araujo, 2005; Perko, Raggam, Deutscher, Gutjahr, & Schardt, 2011) and spaceborne SAR systems (Næsset et al., 2011; Solberg, Astrup, Gobakken, Næsset, & Weydahl, 2010). The satellite SAR mission TanDEM-X (Krieger et al., 2007) acquires single-pass SAR image pairs, which allow DSM generation based on interferometry. The TerraSAR-X mission (Buckreuss, Balzer, Muhlbauer, Werninghaus, & Pitz, 2003) acquires repeat-pass pairs for digital surface model (DSM) generation using radargrammetry. Data from the TanDEM-X and TerraSAR-X missions have produced promising results for estimating volume and biomass (Solberg, Astrup, Breidenbach, Nilsen, & Weydahl, 2013, Solberg, Riegler, & Nonin, 2015). Solberg et al. (2013) found a linear relationship between InSAR height and both biomass and timber volume that allows change estimation without the availability of a DTM.

The accuracy of 3D remote sensing is affected by topography. Earlier studies have found that terrain can influence elevation measurements from ALS (Estornell, Ruiz, Velázquez-Martí, & Hermosilla, 2011; Hodgson & Bresnahan, 2004). Honkavaara, Markelin, Rosnell, and Nurminen (2012) observed larger AP height errors in shaded areas and on forest canopy surfaces with low solar angle. Such errors occur more often on slopes facing away from the sun. As a principally side-looking system, SAR is especially influenced by slope and aspect (Breidenbach, Koch, et al., 2008; Toutin, 2002).

Most studies that have explored 3D remote sensing for forest parameter prediction have analyzed data from one acquisition system. However, in survey planning it is crucial to know about the differences between potential prediction accuracies of remote sensing data. Only with comparable numbers is it possible to find cost-efficient combinations of auxiliary data under the given forest conditions. Previous studies that have compared three or more remote sensing data sets are few in number (e.g. Hyyppä et al., 2000). Moreover, a comparison between different studies is complicated because study design, forest structure, and other factors influence the results.

The aim of our study was therefore to compare four different 3D remote sensing data sets that have the potential of being used in forest inventories in the same study area. In particular, we wanted to quantify the accuracy of ALS, AP, InSAR, and radargrammetry for timber volume estimation. Additionally, we analyzed the influence of topography on the accuracy of the four methods.

2. Material

2.1. Study area and field data

The study area was in Lardal, a municipality in Vestfold County, located in southern Norway on the west side of the Oslofjord (central coordinates: 59.4° North, 9.9° East). The forested area is dominated by Norway spruce (*Picea abies* (L.) Karst.) but also includes stands dominated by Scots pine (*Pinus sylvestris* L.) and broad-leaved tree species (mainly *Betula* spp.; scattered *Sorbus aucuparia*, *Populus tremula*, and *Alnus incana*). The terrain is hilly with altitudes ranging from 50 to 650 m a.s.l. (Fig. 1).

Field data were collected in 2011. From a forest stand map we divided stands into two strata: Stands with a volume >150 m^3 ha^{-1} and stands with a volume < 150 m^3 ha^{-1}. From each of these strata, 20 stands were randomly selected, each of which was 1–3 ha in size. To make the identification of the stands during fieldwork easier only compact stands were considered in the selection. The compactness criterion was

$$\sqrt{A}/P > 0.2 \quad (1)$$

where A is the area and P is the perimeter of the stand. Within each of the selected stands we constructed a 20 m × 20 m grid from which we randomly selected 7 nodes. At these nodes we set the center points of the inventory plots. Only the inventory plots covered by all remote sensing data sets were considered. This resulted in a total of 170 plots located in 25 stands. The spatial distribution of the stands within the study area is shown in Fig. 1b. The plots were located on slopes of 1–30° with a mean of 9° evenly distributed on all aspects. All field measurements were taken in accordance with the Norwegian National Forest Inventory protocol (Tomter, Hylen, & Nilsen, 2010). The circular sample plots had an area of 250 m^2. Diameter at breast height (DBH) and species were recorded for all trees with a DBH > 5 cm. Tree height was measured for a sample of 10 trees per plot. The heights of the remaining trees were estimated using diameter–height models for each plot (Landsskogtakseringen, 2008). Tree stem volumes including bark were estimated using standard models for spruce, pine, and birch (Braastad, 1966; Brantseg, 1967; Vestjordet, 1967). Plot-level stem volume (m^3 ha^{-1}) was obtained by aggregating the single-stem volume estimates. Stand-level stem volume was calculated as the mean volume of the sample plots within the stands. Table 1 lists descriptive statistics for the response variable timber volume. The model-related uncertainties of the volume estimates for the individual plots were assumed to be negligible compared to the between-plot variability and were thus ignored. To ensure an accurate plot location, the center coordinate of all sample plots was measured using a survey-grade differential global positioning system receiver.

Related studies have been conducted in the study area. Korhonen, Kaartinen, Kukko, Solberg, and Astrup (2010) and Breidenbach and Astrup (2014) used the same ALS data, Breidenbach and Astrup (2012) the same AP data, Solberg et al. (2015) the same radargrammetry data, Solberg et al. (2013) a subset of the present InSAR data, and Solberg et al. (2013, 2015) field data from the same forest inventory with a focus on spruce-dominated stands.

2.2. ALS

ALS data were acquired in May 2009 by Blom Geomatics AS, Norway, for the Norwegian Mapping Authority, using two different Optech ALTM Gemini laser scanners mounted on a fixed-wing aircraft. The average flying height was 690 m above ground at an average speed of 80 m s^{-1}. The footprint diameter was 13 cm. The resulting data had an average density of approximately 10 pulses per m^2. The vendor delivered a point cloud containing first, intermediate, and last echoes that were classified as either ground or non-ground echoes.

From the classified ground echoes we created a DTM with a grid cell size of 1 m × 1 m by averaging the height values within each cell using FUSION software (McGaughey, 2013). The DTM was used in all following processing tasks that required ground information, except for the AP data processing.

2.3. AP

Aerial images were acquired in summer 2007 by TerraTec AS, Norway, with a Vexcel UltracamX digital camera. The images had a pan-sharpened ground sampling distance of 20 cm. The within-strip overlap was 60% and the side overlap was 20%. Blom Geomatics AS, Norway, created a DSM with 20 cm × 20 cm grid cell size from the images using SocetSet version 5.5.0 software (BAE Systems) with the NGATE image matching algorithm. A canopy height model (CHM) was created by subtracting a DTM with 1 m × 1 m grid cell size obtained from ALS data derived by the data provider. The CHM was delivered as a raster layer with a grid cell size of 0.2 m × 0.2 m and a vertical resolution of 0.1 m. All negative values in the raster were set to 0. The data have been described in detail by Breidenbach and Astrup (2012).

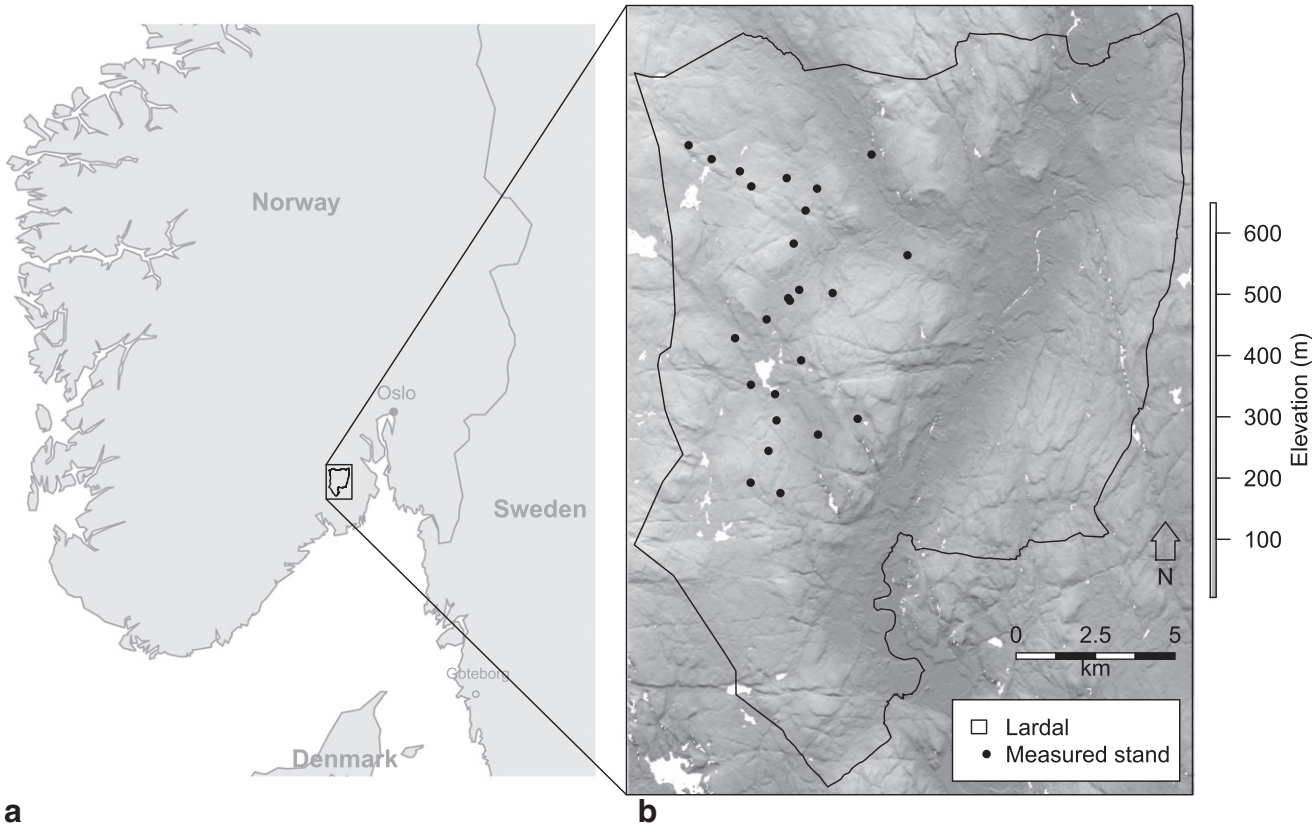

Fig. 1. Overview of the study area (a); terrain and locations of the stands (b).

2.4. InSAR

Three co-registered TanDEM-X StripMap pairs in single look complex format from summer 2011 were used to create the InSAR DSM. Properties of the acquisitions are listed in Table 2. The look direction was always to the right, so that the ascending acquisitions were obtained from a western position relative to the study area and the descending acquisitions from an eastern position. The SARscape 5.0 module of ENVI 5.0 software was used to process the SAR images into DSMs. Using the ALS DTM, differential interferograms were created for every image pair, representing the phase differences caused by vegetation height. After removing random errors with a Boxcar adaptive filter, offset and ramp errors were removed using 30 ground control points. Phase unwrapping was carried out with a 'region growing' method (Reigber & Moreira, 1997). Finally, we converted the unwrapped phases into geocoded DSMs. A CHM was created by subtracting the ALS DTM.

Local coherence γ was calculated within 3 pixel × 3 pixel windows. Since coherence is related to noise and accuracy, it was used as weighting factor in averaging the three CHMs:

$$CHM_{mean} = (\gamma_1\ CHM_1 + \gamma_2\ CHM_2 + \gamma_3\ CHM_3)/(\gamma_1 + \gamma_2 + \gamma_3) \quad (2)$$

where CHM_{mean} is the height of the combined CHMs; CHM_1, CHM_2, and CHM_3 are the CHM heights derived from the three TanDEM-X data sets; and γ_1, γ_2, and γ_3 are the corresponding coherence values. The InSAR-CHM had a grid cell size of 10 m × 10 m.

2.5. Radargrammetry

Six TerraSAR-X StripMap images were acquired over the study area in May 2011. Four of the images were taken in an ascending pass and two in a descending pass (Table 3). The look direction of the sensor was always toward right, so that the images were taken from a western and eastern point of view during ascending and descending passes, respectively. The images were grouped into three stereo pairs with intersection angles of 16°, 15°, and 21°, respectively. We used 3 pairs of images for both InSAR and radargrammetry, in order to make the performance of the two technologies comparable. Each of the TerraSAR-X stereo pairs was processed into a radargrammetry DSM using a SAR stereo-matching algorithm developed by the vendor, EADS Astrium (Solberg et al., 2015). The three DSMs were merged to a single DSM by averaging. This step reduced random errors and errors from shadowing, foreshortening, and layover. Small voids (up to 8 pixels) were filled by mean value interpolation using the 8 neighboring pixels.

Table 1
Summary of field data for the 170 field plots (m^3 ha^{-1}).

Variable	Plot level			Stand level		
	Mean	Std.dev	Maximum	Mean	Std.dev	Maximum
Total volume	186.45	130.70	596.00	185.18	105.64	364.71
Spruce volume	153.40	129.50	596.00	151.78	101.87	338.71
Pine volume	13.37	35.80	267.00	13.83	24.70	80.00
Broad-leaved species volume	19.68	33.93	199.00	19.58	19.21	67.86

Table 2
Characteristics of the TanDEM-X acquisitions for InSAR.

Acquisition date	Pass[a]	Incidence angle (°)	Normal baseline (m)	Height of ambiguity (m)
23 July 2011	Asc	36	251	23
05 Sept 2011	Asc	36	238	24
01 Sept 2011	Desc	43	59	122

[a] Asc = ascending pass, Desc = descending pass.

Table 3
Characteristics of the TerraSAR-X acquisitions for radargrammetry.

Pair	Acquisition date	Pass[a]	Incidence angle (°)
1	07 May 2011	Asc	35
1	06 May 2011	Asc	52
2	18 May 2011	Asc	37
2	17 May 2011	Asc	53
3	14 May 2011	Desc	44
3	13 May 2011	Desc	21

[a] Asc = ascending pass, Desc = descending pass

Single pixels with a height difference of ±20 m compared to the surrounding pixels were automatically detected and removed. Approximately 100 linear artifacts that occurred at the scene edges were manually corrected. The DSM had a grid cell size of 10 m × 10 m and a vertical resolution of 1 m. A CHM was created by subtracting the ALS DTM.

3. Methods

3.1. Computation of explanatory variables

3.1.1. ALS and AP

To acquire height above ground (m) for the ALS data we subtracted the corresponding terrain height of the ALS DTM from the heights of the ALS echoes. The AP data were already delivered as heights above ground (m) by the vendor, who used an ALS-derived DTM (Breidenbach & Astrup, 2012). From these data we derived metrics describing the height distribution of each sample plot. The selection of metrics followed Næsset (2004), with the exception that also echoes with height <2 m were considered in the calculation. No other height limit was applied to select echoes for the calculation of metrics. 9 different metrics were calculated: height percentiles for 10%, 50%, and 90% (denoted p_{10}, p_{50}, p_{90}, respectively); maximum, mean, and coefficient of variation (h_{max}, h_{mean}, h_{CV}); and canopy density metrics, which were created by dividing the height between minimum and maximum height by 10 and calculating the proportion of echoes above the vertical parts #1, #5, and #9 (d_1, d_5, d_9). From the ALS data, the above-described metrics were computed separately from three echo categories: all echoes, first and single echoes, and last echoes. This resulted in a total of 27 metrics for ALS and 9 metrics for AP. For ALS we used the notation $p_{10\,a}$, $p_{50\,a}$, $p_{90\,a}$, $h_{max\,a}$, $h_{mean\,a}$, $h_{CV\,a}$, $d_{1\,a}$, $d_{50\,a}$, $d_{9\,a}$; $p_{10\,f}$, $p_{50\,f}$, $p_{90\,f}$, $h_{max\,f}$, $h_{mean\,f}$, $h_{CV\,f}$, $d_{1\,f}$, $d_{5\,f}$, $d_{9\,f}$; $p_{10\,l}$, $p_{50\,l}$, $p_{90\,l}$, $h_{max\,l}$, $h_{mean\,l}$, $h_{CV\,l}$, $d_{1\,l}$, $d_{5\,l}$, $d_{9\,l}$, where a = metrics derived from all echoes, f = metrics derived from first and single echoes, and l = metrics derived from last echoes.

3.1.2. InSAR and radargrammetry

From the InSAR and radargrammetric CHMs, mean heights (m) were calculated for use as explanatory variables in the models. For each plot, intersecting pixels of the CHM were weighted by their intersection area:

$$h_{mean} = (h_1a_1 + h_2a_2 + \ldots + h_ia_i)/(a_1 + a_2 + \ldots + a_i) \quad (3)$$

where h_i is the height of the ith pixel covering a sample plot and a_i is the intersection area of that pixel. A maximum of $i = 9$ pixels could cover a sample plot.

3.2. Modeling

Linear mixed effects models were fitted to each of the four remote sensing data sets. Plot-level timber volume was the response variable and the metrics derived from the remote sensing data served as candidate explanatory variables. To account for the hierarchical field sample design we introduced a random intercept at stand level. Heteroscedasticity was handled by introducing a variance function based on a mean-height metric (ALS: $h_{mean\,a}$; AP, InSAR, radargrammetry: h_{mean}).

For ALS and AP data we identified relevant fixed effects using a stepwise forward variable selection algorithm minimizing the Bayesian information criterion (BIC). In addition to the derived metrics, their quadratic terms were added to the pool of candidate explanatory variables to allow potential nonlinearities in the data. Subsequently, the importance of the selected variables was analyzed in a backward elimination based on the cross-validated root mean squared error at plot level ($RMSE_{plot}$, see (Eq. 5)). If the removal of a variable improved the RMSE, the variable was omitted from the final model. The resulting models were formulated as

$$\begin{aligned} &y_{ij} = \beta_0 + b_i + \beta_1 x_{ij1} + \beta_2 x_{ij2} + \ldots + \beta_k x_{ijk} + \varepsilon_{ij} \\ &i = 1, \ldots, m \quad j = 1, \ldots, n_i \quad b_i \sim N\left(0, \sigma_b^2\right) \quad \varepsilon_{ij} \sim N\left(0, \sigma_\varepsilon^2 \upsilon_{ij}^{2\delta}\right) \end{aligned} \quad (4)$$

where y_{ij} is the observed volume of the jth sample plot in the ith stand, $x_{ij1}, \ldots, x_{ijk}$ are the k fixed effects, $\beta_0, \ldots, \beta_k$ are the fixed parameters, n_i is the number of sample plots within stand i, and m is the number of forest stands. We assumed that the stand-level random effects b_i were independent of the plot-level residuals ε_{ij}. The variance in the random effect is denoted σ_b^2. $\sigma_\varepsilon^2 \upsilon_{ij}^{2\delta}$ is the variance function to model the heteroscedasticity in the residual errors with δ as the variance parameter and the metric $h_{mean\,a}$ or h_{mean}, respectively, as the variance covariate υ. Similarly, linear mixed effects models were fitted for the InSAR and radargrammetry data sets. The explanatory variable in the models was the h_{mean} of the InSAR and radargrammetric CHM. It was analyzed if the addition of the quadratic term h_{mean}^2 reduced the cross-validated plot-level RMSE. The models for the SAR data were in accordance with Eq. (4).

For all statistical computations we used the R software for statistical computing (R Core Team, 2013), expanded with the package nlme (Pinheiro, Bates, DebRoy, Sarkar, & R Core Team, 2013) for mixed effects modeling. Following Breidenbach, Koch, et al. (2008), who observed spatial dependencies between sample plot residuals, we investigated within-stand spatial autocorrelation by visual analysis of variograms of the model residuals implemented in the nlme package.

We calculated the RMSE at plot level by leave-one-stand-out cross-validation (LOSOCV):

$$RMSE_{plot} = \sqrt{\frac{1}{\sum_{i=1}^{m} n_i} \sum_{i=1}^{m} \sum_{j=1}^{n_i} \left(y_{ij} - \tilde{y}_{ij}\right)^2} \quad (5)$$

where $\tilde{y}_{ij}$ is the predicted timber volume, using the fixed effects of the model Eq. (4), at plot j when omitting all plots in stand i for the model fit.

To compare the accuracy of the remote sensing methods at stand level, we aggregated the plot-level observations and LOSOCV predictions within each stand. Aggregation of field plots has the advantage that stand-level field observations are available rather than estimates. The disadvantage is that the stands only consist of the area covered by 5–7 sample plots and are therefore rather small. Eq. (6) was used to compute the RMSE of the mean volume estimates at stand level.

$$RMSE_{stand} = \sqrt{\frac{1}{m} \sum_{i=1}^{m} \left(\frac{1}{n_i} \sum_{j=1}^{n_i} \left(y_{ij} - \tilde{y}_{ij}\right)^2 \right)} \quad (6)$$

Subsequently, the relative RMSE of plot and stand level in percent was calculated as:

$$RMSE[\%] = \frac{RMSE}{\bar{y}} \times 100 \quad (7)$$

where $\bar{y}$ is the arithmetic mean timber volume of all plots.

3.3. Terrain influence

To test the terrain influence on the prediction accuracy we calculated slope and aspect of the terrain at every sample plot, based on the ALS DTM. For each sample plot, we cut the DTM to a 60 m × 60 m area around the plot center and resampled it to a grid cell size of 20 m × 20 m, so that every sample plot was covered by a single DTM raster cell centered on the plot. In this way we obtained a single value for slope and aspect using an algorithm by Horn (1981) for each sample plot. For a visual assessment the LOSOCV model residuals were plotted against slope and aspect. The same was done with relative residuals $\left(\left(y_{ij}-\tilde{y}_{ij}\right)/y_{ij}\right)$ to eliminate the effect of the magnitude of the response variable. To analyze interaction between slope and aspect we also plotted the residuals of stands on slopes of more than 10° against aspect.

Subsequently, a statistical analysis was performed. Aspect was converted into a categorical variable where 0–45° and 315–360° was north, 45–135° was east, 135–225° was south, and 225–315° was west. We included the terrain properties slope and aspect of the sample plots in the previously selected models of each data set. The first model contained the variable slope (slope model). The second model contained slope and a slope–aspect interaction term (slope–aspect model). It was considered meaningless to fit a model containing the variable aspect as single term, since an aspect-dependent intercept on near-horizontal slopes does not make sense. Likelihood-ratio tests were used to compare the original model and the two models incorporating terrain properties. For likelihood ratio testing, all three models were fitted using maximum likelihood estimation. A final analysis of the terrain influence was performed by calculating the relative LOSOCV RMSE of the slope–aspect model and comparing it with the plot-level RMSE of the original model.

4. Results

4.1. Prediction models

For ALS, four explanatory variables were selected using the stepwise forward selection algorithm based on the BIC. The selected variables were the height metric $h_{mean\ f}$, the quadratic terms $h^2_{mean\ a}$ and $p^2_{90\ a}$, and the density metric $d^2_{9\ f}$. The metric $h^2_{mean\ a}$ was removed in the backward elimination. For AP, the stepwise forward selection algorithm identified the height metrics h_{mean} and p^2_{50}, and the density metric d^2_1 as influential variables. However, a lower RMSE was achieved when p^2_{50} was removed during backward selection. The InSAR and the radargrammetry models were fitted with the mean CHM height h_{mean} as the only predictor variable. The quadratic term h^2_{mean} did not decrease the RMSE in either model and was therefore not included. Details of the models are listed in Table 4.

Fig. 2 shows observed timber volume plotted against the corresponding predictions from the remote sensing models. The smallest deviation from the 1:1 line is visible in the ALS model scatterplot, followed by the AP model scatterplot with larger residuals in the stands with the highest observed volume. The variability in the residuals of InSAR and radargrammetry was generally higher than for the other remote sensing methods. The heteroscedasticity was considered using variance models. There was no indication of spatial autocorrelation of the residuals within the stands when considering the random effect on stand level.

The LOSOCV RMSEs of the models are presented in Table 5. The aggregation resulted in the underestimation of the stand with the highest timber volume. While five plots within that stand were underestimated with all remote sensing data sets, the underestimation was most severe with the AP data. Additionally, the remaining two plots were close to the 1:1 line in AP, as opposed to the InSAR and radargrammetry predictions where they reduced the underestimation. In AP the absolute residual of the stand was three times bigger than the standard deviation of all residuals. No error was found in the field or remote sensing data. When omitting the stand, the RMSEs on stand level were 12% for ALS, 13% for AP, 19% for InSAR, and 25% for radargrammetry.

Table 4
Variables and parameter estimates of the linear mixed models.

Remote sensing data set	Variable[a]	Estimate[b]	Standard deviation
ALS			
	Intercept	-2.82^{ns}	3.68
	$h_{mean\ f}$	26.20^{***}	1.42
	$p^2_{90\ a}$	0.33^{***}	0.05
	$d^2_{9\ f}$	-9042.60^{**}	2684.09
	δ	0.91	
	σ_b		11.15
AP			
	Intercept	23.27^{**}	8.11
	h_{mean}	24.73^{***}	1.21
	d^2_1	-47.93^{***}	14.10
	δ	0.39	
	σ_b		18.26
InSAR			
	Intercept	1.42^{ns}	10.67
	h_{mean}	27.04^{***}	1.60
	δ	0.35	
	σ_b		17.78
Radargrammetry			
	Intercept	12.25^{ns}	14.52
	h_{mean}	23.16^{***}	1.80
	δ	0.26	
	σ_b		29.21

[a] δ is the variance parameter in the variance function $\sigma^2_\varepsilon v^{2\delta}_{ij}$.
[b] With level-of-significance of t-tests (*** p < 0.001, ** p < 0.01, * p < 0.05; ^{ns} p > 0.05).

To show the potential of the different data sets for practical application and to visualize the timber volume prediction accuracy we created wall-to-wall prediction maps for a subset of the test area using each of the data sets. Fig. 3 shows the prediction maps based on the fitted models. While in the InSAR map the open areas are recognizable, only the high volume area is apparent at the central eastern border of the radargrammetry map.

4.2. Terrain influence

The analysis of terrain influence did not give consistent results for all data sets. The visual assessment of aspect and slope revealed no obvious trends or patterns in the residuals. However, the statistical analysis revealed the influence of slope and aspect. The results of the likelihood ratio tests are given in Table 6. Agreeing on the common level of significance of 0.05, the p-values showed that the inclusion of slope and the interaction term of slope and aspect provided a significantly better model fit for AP and InSAR. Slope alone was not significant when included in any of the four original models. Additionally, the slope decreased the RMSE of the AP, InSAR, and radargrammetry models, while no change was observed for ALS (Table 7). Taken together, there was an influence of terrain on timber volume prediction with AP, InSAR and radargrammetry even though the RMSEs decreased by less than 1 percentage point. The results of the analysis suggested that the only predictions not influenced by topography were the ALS predictions.

Table 8 shows the change in predicted timber volume when slope is increased by 1° and all other parameters remain the same. The slope–aspect models of the SAR data sets show a strong negative impact of eastern slopes and a positive impact of western and southern slopes. The slope–aspect model of AP behaves differently. It shows a positive slope impact on southern and eastern slopes and a negative impact on western and northern slopes.

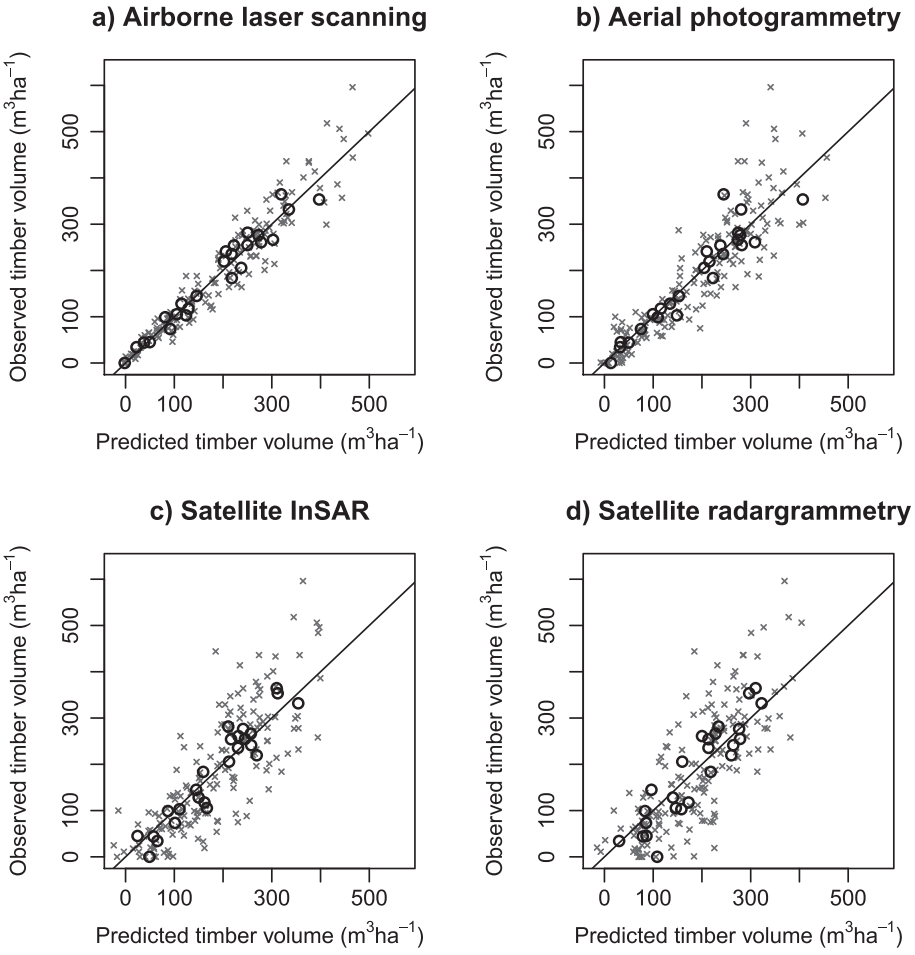

Fig. 2. Observed versus predicted (LOSOCV) timber volume for all fitted models; crosses = sample plots; circles = stand means.

5. Discussion

In our study we quantified the accuracy of timber volume estimation based on ALS, AP, InSAR, and radargrammetry. At plot level the RMSEs suggested the following accuracy ranking, starting with the highest accuracy: ALS, AP, InSAR, radargrammetry. At stand level the RMSE of AP was slightly higher than the RMSE of InSAR. This was caused by one outlying stand in the AP predictions. Taking the scatterplots and the influence of the largely underpredicted stand into account, the accuracy ranking at plot level is also valid at stand level.

Earlier studies compared only one or two different 3D remote sensing data sets for the same study area. We tried to relate our results to some of those studies to verify the achieved accuracies in order to generalize our results. Comparisons of RMSEs between studies are problematic, since different study designs, forest structure, and study site properties lead to different results. An important factor that must be considered is the sample plot size, since standard errors decrease with increasing plot size (Mascaro, Detto, Asner, & Muller-Landau, 2011; Næsset, 2002b). The decrease becomes visible when comparing the plot-level RMSEs to the stand-level RMSEs.

Table 5
LOSOCV RMSEs of the timber volume prediction.

Remote sensing data set	Plot-level RMSE		Stand-level RMSE	
	(m^3ha^{-1})	(%)	(m^3ha^{-1})	(%)
ALS	36.20	19.42	23.05	12.36
AP	58.59	31.43	33.79	18.12
InSAR	77.56	41.60	33.74	18.10
Radargrammetry	82.82	44.42	43.38	23.27

The RMSE of our ALS model was similar to the findings of Breidenbach and Astrup (2014) and in the ranges Næsset et al. (2004) reported for stem volume estimation models in the Nordic Countries, which were 15–25% at plot level and 9–43% at stand level. Järnstedt et al. (2012) obtained an RMSE of 31% for timber volume estimation with ALS data and 40% with AP data for 300 m^2 plots. In the same area and with similar field data Vastaranta et al. (2013) achieved a plot-level RMSE of 18% and 25% with ALS and AP, respectively. They explain the difference compared to the findings by Järnstedt et al. (2012) as being due to a higher sample plot number, higher field measurement means, and a different estimation technique. Straub et al. (2013) obtained an RMSE at plot level of 34% and 41% with ALS (first and last echoes) and AP respectively, for 500 m^2 plots. Taken together, the above-mentioned studies identified that models based on ALS data produce more accurate predictions than models based on AP. By contrast, Nurminen et al. (2013) and Bohlin et al. (2012) reported similar accuracies for estimations based on ALS and AP. Nurminen et al. (2013) achieved an RMSE of 21% with ALS and 23% with AP for plots of various sizes with a mean of 390 m^2. On stand level Bohlin et al. (2012) obtained an RMSE of 13% for volume predictions with AP and compared it to an earlier ALS study in the same area that had obtained an RMSE of 11% (Holmgren, 2004). Our findings correspond to those from both of the aforementioned studies. Although the AP data were delivered as a raster representing a smoothed surface, we treated ALS and AP data in the same way. The use of a raw point cloud of matched points might improve the accuracy of the AP predictions.

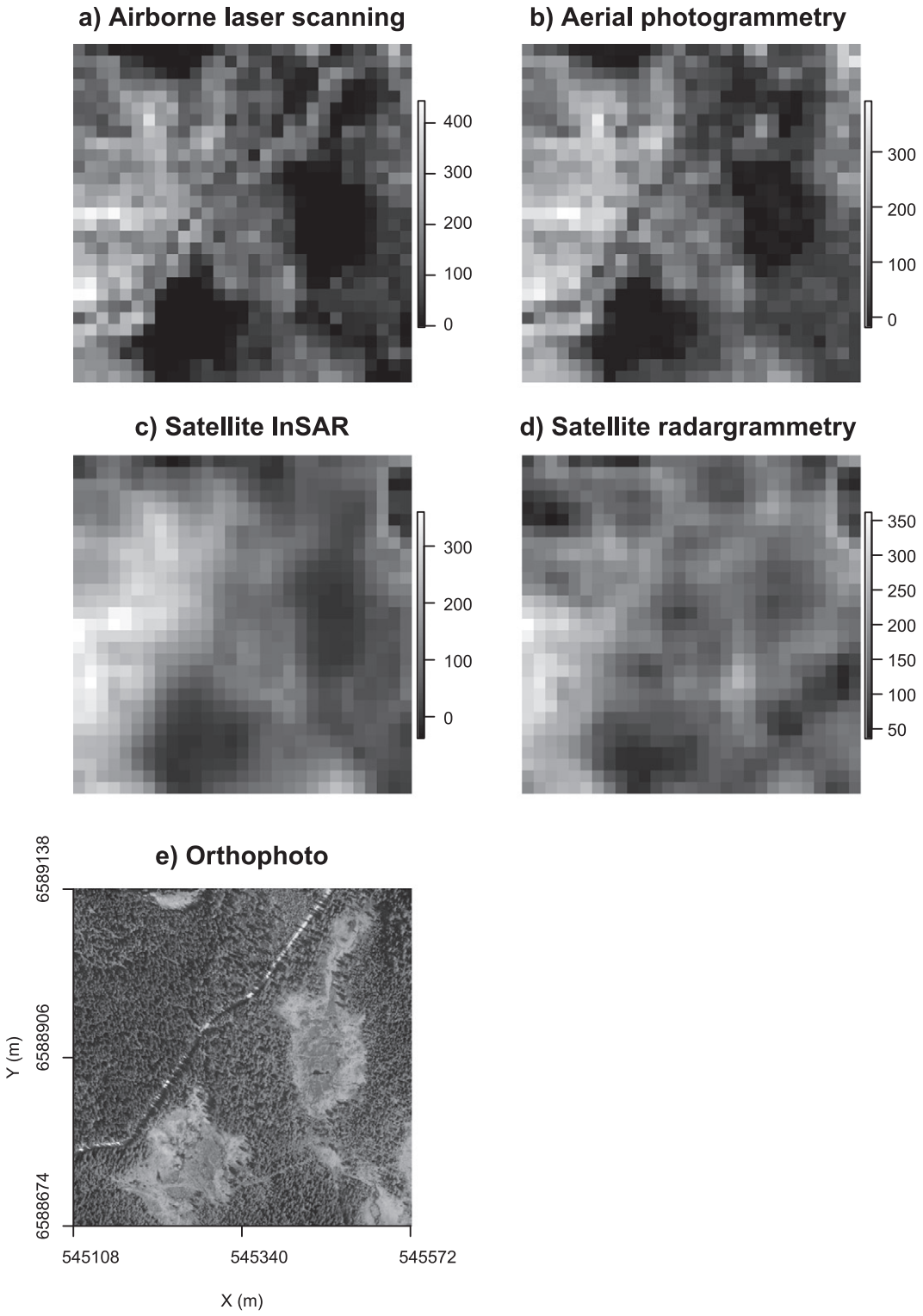

Fig. 3. Timber volume prediction maps (m^3 ha^{-1}) derived from the four remote sensing data sets (a–d), and orthophoto (e) for a subset of the test area; the coordinate system is UTM zone 32 N.

Solberg et al. (2013) combined two TanDEM-X InSAR DSMs to estimate timber volume in spruce-dominated stands for a slightly larger study area than ours, which also included the present data. They reported a relative RMSE of 44% for 250 m^2 plots and 20% for stands. Comparable to our study, Næsset et al. (2011) evaluated the performance of ALS and Shuttle Radar Topography Mission (SRTM) InSAR for above-ground biomass area estimates. They achieved standard errors of 1.6 and 3.2 Mg ha^{-1} using ALS and InSAR respectively, which supports our finding that the InSAR RMSE is approximately twice as high as the ALS RMSE. To date, few studies have compared radargrammetry with other remote sensing systems for forest parameter estimation. Solberg et al. (2015) used TerraSAR-X radargrammetry data to estimate timber volume in spruce-dominated stands in the same study area. In common with our results, they achieved a relative plot-level RMSE of 42% and a

Table 6
Results of likelihood ratio tests comparing the initially selected models with models incorporating slope and the interaction term of slope and aspect of the sample plots.

Remote sensing data set	Compared model	Degrees of freedom	Likelihood ratio	p-value
ALS	Slope model	8	0.07	0.793
	Slope–aspect model	11	6.30	0.178
AP	Slope model	7	1.23	0.267
	Slope–aspect model	10	11.92	0.018
InSAR	Slope model	6	0.00	0.969
	Slope–aspect model	9	17.95	0.001
Radargrammetry	Slope model	6	0.03	0.867
	Slope–aspect model	9	7.13	0.129

stand-level RMSE of 18%. One reason for the larger prediction errors with both SAR systems compared to ALS and AP may be their larger grid cell size.

In contrast to Breidenbach, Kublin, et al. (2008), who fitted mixed effects models to predict timber volume from ALS, no influential spatial autocorrelation in the residuals within stands was found in our study. Thus, the stands' homogeneity is such that the random effect covers the natural spatial autocorrelation. This is particularly important for SAR data because distances between sample plot boundaries are sometimes smaller than the grid cell size of the SAR CHMs. The absence of spatial autocorrelation simplifies the estimation of stand-level variance estimates (McRoberts, Næsset, & Gobakken, 2013).

The analysis of the terrain influence showed that the inclusion of slope and aspect in prediction models can improve the accuracy of timber volume predictions. The RMSEs of the AP, InSAR, and radargrammetry models decreased by less than 1 percentage point, which may be marginal for practical applications. The results indicate that of all compared methods, InSAR predictions are affected most by topography. Correspondingly, Breidenbach, Koch, et al. (2008) found that aspect had a strong effect on mean tree height estimates based on InSAR data. While they used only one scene, we combined ascending and descending acquisitions to generate a DSM, which presumably moderated the effects of slope and aspect. Future studies using InSAR data on rugged terrain should pay attention to these effects. The similar behavior of the SAR slope–aspect models on eastern, southern, and western slopes might be caused by the SAR-specific geometry resulting in layover, foreshortening, and shadowing. Since AP is derived from a passive sensor, the impact of slope and aspect is likely caused by solar elevation during image acquisition.

The results of our study are relevant to inform data selection decisions in forest survey planning when using remote sensing data for forest parameter prediction. Næsset et al. (2011) indicated how the field costs of a forest inventory might change when using different remote sensing data. They estimated that in order to achieve the same precision in an overall biomass estimate for their study area the number of field plots could be reduced by approximately 80% when using ALS data to support the estimation compared to a pure field survey with no use of remote sensing data. Similarly, there was a 25% reduction in the required field plot numbers when using InSAR data from SRTM.

Our analysis was solely based on the 3D information contained in the data sets. We did not consider other information that could have improved timber volume predictions, such as intensity values in ALS data (Ørka et al., 2009) or coherence in SAR data (Balzter, 2001; Schlund, von Poncet, Hoekman, Kuntz, & Schmullius, 2014). A known potential lies in the color information of AP data, which presumably can be used for tree species specific estimations of forest attributes. Additionally, special properties of remote sensing systems might outweigh higher prediction accuracy. An example is the capacity of SAR systems to acquire images under cloudy conditions.

Table 7
Relative LOSOCV RMSEs of slope–aspect models compared to initial models.

Remote sensing data set	Initial model	Slope–aspect model	ΔRMSE
	RMSE (%)	RMSE (%)	(percentage points)
ALS	19.42	19.43	−0.01
AP	31.43	30.76	0.67
InSAR	41.60	40.62	0.98
Radargrammetry	44.42	43.87	0.55

Table 8
Change of predicted timber volume when slope is increased by 1° and all other parameters remain the same.

Remote sensing data set	Timber volume change (m^3 ha^{-1})			
	North	East	South	West
AP	−0.489	0.582	1.636	−1.890
InSAR	1.962	−2.816	0.773	2.428
Radargrammetry	−0.284	−2.204	1.754	1.181

6. Conclusions

Common types of 3D remote sensing data were compared on a single test site using the same reference data and methods. Therefore we were able to rank the data sets based on their prediction accuracy. While ALS provided the most accurate predictions, we observed higher errors with the other airborne system, AP. At plot level, the InSAR RMSE was approximately twice as high as the ALS RMSE. Radargrammetry showed a slightly lower accuracy than InSAR. Aggregation at stand level decreased the RMSE by 36–56%. Additionally, we conclude that terrain has a significant but marginal influence on the prediction accuracy of AP, InSAR, and radargrammetry.

Acknowledgments

The authors are grateful to the anonymous reviewers whose comments greatly helped to improve the clarity and precision of the paper. We acknowledge Deutsches Zentrum für Luft und Raumfahrt (DLR) for the provision of TanDEM-X science data free of charge.

References

Balzter, H. (2001). Forest mapping and monitoring with interferometric synthetic aperture radar (InSAR). *Progress in Physical Geography*, *25*(2), 159–177.
Bohlin, J., Wallerman, J., & Fransson, J. (2012). Forest variable estimation using photogrammetric matching of digital aerial images in combination with a high-resolution DEM. *Scandinavian Journal of Forest Research*, *27*(7), 692–699.
Braastad, H. (1966). Volume tables for birch. *Norwegian with English summary. Meddr. Norske SkogforsVes., Oslo.* (pp. 265–365).
Brantseg, A. (1967). Volume functions and tables for Scots pine. South Norway. *Norwegian with English summary. Meddr. Norske SkogforsVes.* (pp. 695–739).
Breidenbach, J., & Astrup, R. (2012). Small area estimation of forest attributes in the Norwegian National Forest Inventory. *European Journal of Forest Research*, *1–13*.
Breidenbach, J., & Astrup, R. (2014). The semi-individual tree crown approach. *Forestry applications of airborne laser scanning* (pp. 113–133). Springer.
Breidenbach, J., Koch, B., Kändler, G., & Kleusberg, A. (2008). Quantifying the influence of slope, aspect, crown shape and stem density on the estimation of tree height at plot level using lidar and InSAR data. *International Journal of Remote Sensing*, *29*(5), 1511–1536.
Breidenbach, J., Kublin, E., McGaughey, R., Andersen, H. -E., & Reutebuch, S. (2008). Mixed-effects models for estimating stand volume by means of small footprint airborne laser scanner data. *Photogrammetric Journal of Finland*, *21*(1), 4–15.
Buckreuss, S., Balzer, W., Muhlbauer, P., Werninghaus, R., & Pitz, W. (2003). The TerraSAR-X satellite project. *Geoscience and remote sensing symposium, 2003. IGARSS'03. Proceedings. 2003 IEEE International, Vol. 5.* (pp. 3096–3098). IEEE.
Estornell, J., Ruiz, L. A., Velázquez-Martí, B., & Hermosilla, T. (2011). Analysis of the factors affecting LiDAR DTM accuracy in a steep shrub area. *International Journal of Digital Earth*, *4*(6), 521–538.
Hodgson, M. E., & Bresnahan, P. (2004). Accuracy of airborne lidar-derived elevation: Empirical assessment and error budget. *Photogrammetric Engineering and Remote Sensing*, *70*(3), 331–340.
Holmgren, J. (2004). Prediction of tree height, basal area and stem volume in forest stands using airborne laser scanning. *Scandinavian Journal of Forest Research*, *19*(6), 543–553.
Honkavaara, E., Markelin, L., Rosnell, T., & Nurminen, K. (2012). Influence of solar elevation in radiometric and geometric performance of multispectral photogrammetry. *ISPRS Journal of Photogrammetry and Remote Sensing*, *67*, 13–26.

Horn, B. K. (1981). Hill shading and the reflectance map. *Proceedings of the IEEE*, *69*(1), 14–47.
Hugershoff, R. (1933). Die photogrammetrische Vorratsermittlung. *Tharandter Forstliches Jahrb*, *84*, 159–166.
Hyyppä, J., Hyyppä, H., Inkinen, M., Engdahl, M., Linko, S., & Zhu, Y. (2000). Accuracy comparison of various remote sensing data sources in the retrieval of forest stand attributes. *Forest Ecology and Management*, *128*(1), 109–120.
Järnstedt, J., Pekkarinen, A., Tuominen, S., Ginzler, C., Holopainen, M., & Viitala, R. (2012). Forest variable estimation using a high-resolution digital surface model. *ISPRS Journal of Photogrammetry and Remote Sensing*, *74*, 78–84.
Korhonen, L., Kaartinen, H., Kukko, A., Solberg, S., & Astrup, R. (2010). Estimating vertical canopy cover with terrestrial and airborne laser scanning. *10th International Conference on LiDAR Applications for Assessing Forest Ecosystems (Silvilaser 2010)*.
Krieger, G., Moreira, A., Fiedler, H., Hajnsek, I., Werner, M., Younis, M., et al. (2007). TanDEM-X: A satellite formation for high-resolution SAR interferometry. *IEEE Transactions on Geoscience and Remote Sensing*, *45*(11), 3317–3341.
Landsskogtakseringen (2008). *Landsskogtakseringens feltinstruks 2008*. Håndbok fra Skog og landskap 05/08. Norway: Skog og landskap, Ås.
Leberl, F., Irschara, A., Pock, T., Meixner, P., Gruber, M., Scholz, S., et al. (2010). Point Clouds: Lidar versus 3D Vision. *Photogrammetric Engineering & Remote Sensing*, *76*(10), 1123–1134.
Maltamo, M., & Packalen, P. (2014). Species-specific management inventory in Finland. *Forestry Applications of Airborne Laser Scanning* (pp. 241–252). Springer.
Mascaro, J., Detto, M., Asner, G. P., & Muller-Landau, H. C. (2011). Evaluating uncertainty in mapping forest carbon with airborne LiDAR. *Remote Sensing of Environment*, *115*(12), 3770–3774.
McGaughey, R. (2013). FUSION/LDV: Software for LIDAR Data Analysis and Visualization. *Tech. rep., USDA, Pacific North-West Research Center, Seattle, USA*.
McRoberts, R. E., Næsset, E., & Gobakken, T. (2013). Inference for lidar-assisted estimation of forest growing stock volume. *Remote Sensing of Environment*, *128*, 268–275.
McRoberts, R. E., Tomppo, E. O., & Næsset, E. (2010). Advances and emerging issues in national forest inventories. *Scandinavian Journal of Forest Research*, *25*(4), 368–381.
Næsset, E. (2002a). Determination of mean tree height of forest stands by digital photogrammetry. *Scandinavian Journal of Forest Research*, *17*(5), 446–459.
Næsset, E. (2002b). Predicting forest stand characteristics with airborne scanning laser using a practical two-stage procedure and field data. *Remote Sensing of Environment*, *80*(1), 88–99.
Næsset, E. (2004). Effects of different flying altitudes on biophysical stand properties estimated from canopy height and density measured with a small-footprint airborne scanning laser. *Remote Sensing of Environment*, *91*(2), 243–255.
Næsset, E. (2014). Area-based inventory in Norway—from innovation to an operational reality. *Forestry Applications of Airborne Laser Scanning* (pp. 215–240). Springer.
Næsset, E., Gobakken, T., Holmgren, J., Hyyppä, H., Hyyppä, J., Maltamo, M., et al. (2004). Laser scanning of forest resources: The Nordic experience. *Scandinavian Journal of Forest Research*, *19*(6), 482–499.
Næsset, E., Gobakken, T., Solberg, S., Gregoire, T., Nelson, R., Ståhl, G., et al. (2011). Model-assisted regional forest biomass estimation using LiDAR and InSAR as auxiliary data: A case study from a boreal forest area. *Remote Sensing of Environment*, *115*(12), 3599–3614.
Neeff, T., Dutra, L., dos Santos, J., da Costa Freitas, C., & Araujo, L. (2005). Tropical forest measurement by interferometric height modeling and P-band radar backscatter. *Forest Science*, *51*(6), 585.
Nurminen, K., Karjalainen, M., Yu, X., Hyyppä, J., & Honkavaara, E. (2013). Performance of dense digital surface models based on image matching in the estimation of plot-level forest variables. *ISPRS Journal of Photogrammetry and Remote Sensing*, *83*, 104–115.
Ørka, H., Næsset, E., & Bollandsås, O. (2009). Classifying species of individual trees by intensity and structure features derived from airborne laser scanner data. *Remote Sensing of Environment*, *113*(6), 1163–1174.
Perko, R., Raggam, H., Deutscher, J., Gutjahr, K., & Schardt, M. (2011). Forest assessment using high resolution SAR data in X-band. *Remote Sensing*, *3*(4), 792–815.
Pinheiro, J., Bates, D., DebRoy, S., Sarkar, D., & R Core Team (2013). *nlme: Linear and nonlinear mixed effects models*. R package version 3.1-111.
R Core Team (2013). *R: A language and environment for statistical computing*. Vienna, Austria: R Foundation for Statistical Computing (URL http://www.R-project.org).
Reigber, A., & Moreira, J. (1997). Phase unwrapping by fusion of local and global methods. *Geoscience and Remote Sensing, 1997. IGARSS'97. Remote Sensing—A Scientific Vision for Sustainable Development., 1997 IEEE International, Vol. 2*. (pp. 869–871). IEEE.
Schardt, M., Hruby, W., Hirschmugl, M., Wack, R., & Franke, M. (2004). Comparison of aerial photographs and laser scanning data as methods for obtaining 3D forest stand parameters. *Proc. of the ISPRS working group VII/2 — laser-scanners for forest and landscape assessment* (pp. 272–276).
Schlund, M., von Poncet, F., Hoekman, D. H., Kuntz, S., & Schmullius, C. (2014). Importance of bistatic SAR features from TanDEM-X for forest mapping and monitoring. *Remote Sensing of Environment*, *151*, 16–26.
Solberg, S., Astrup, R., Breidenbach, J., Nilsen, B., & Weydahl, D. (2013). Monitoring spruce volume and biomass with InSAR data from TanDEM-X. *Remote Sensing of Environment*, *139*, 60–67.
Solberg, S., Astrup, R., Gobakken, T., Næsset, E., & Weydahl, D. J. (2010). Estimating spruce and pine biomass with interferometric X-band SAR. *Remote Sensing of Environment*, *114*(10), 2353–2360.
Solberg, S., Riegler, G., & Nonin, P. (2015). Estimating forest biomass from TerraSAR-X stripmap radargrammetry. *IEEE Transactions on Geoscience and Remote Sensing*, *53*(1), 154–161.
Steinmann, K., Mandallaz, D., Ginzler, C., & Lanz, A. (2013). Small area estimations of proportion of forest and timber volume combining Lidar data and stereo aerial images with terrestrial data. *Scandinavian Journal of Forest Research*, *28*(4), 373–385.
Straub, C., Stepper, C., Seitz, R., & Waser, L. T. (2013). Potential of UltraCamX stereo images for estimating timber volume and basal area at the plot level in mixed European forests. *Canadian Journal of Forest Research*, *43*(8), 731–741.
Tomter, S., Hylen, G., & Nilsen, J. -E. (2010). *National forest inventories: Pathways for common reporting*. Springer Verlag, Ch. Norways national forest inventory.
Toutin, T. (2002). Impact of terrain slope and aspect on radargrammetric DEM accuracy. *ISPRS Journal of Photogrammetry and Remote Sensing*, *57*(3), 228–240.
Toutin, T., & Gray, L. (2000). State-of-the-art of elevation extraction from satellite SAR data. *ISPRS Journal of Photogrammetry and Remote Sensing*, *55*(1), 13–33.
Treuhaft, R., & Siqueira, P. (2000). Vertical structure of vegetated land surfaces from interferometric and polarimetric radar. *Radio Science*, *35*(1), 141–177.
Vastaranta, M., Wulder, M.A., White, J. C., Pekkarinen, A., Tuominen, S., Ginzler, C., et al. (2013). Airborne laser scanning and digital stereo imagery measures of forest structure: Comparative results and implications to forest mapping and inventory update. *Canadian Journal of Remote Sensing*, *39*(05), 1–14.
Vestjordet, E. (1967). Functions and tables for volume of standing trees. Norway spruce. *Norwegian with English summary. Meddr. Norske SkogforsVes*. (pp. 543–574).